Article

Refractive Index Sensor Based on Metal–Insulator–Metal Waveguide Coupled with Symmetric Structure

Shubin Yan[1,†,*], Meng Zhang[1,†], Xuefeng Zhao [1], Yanjun Zhang [1], Jicheng Wang [2] and Wen Jin [3]

[1] Science and Technology on Electronic Test and Measurement Laboratory, North University of China, No. 3 Xueyuan Road, Taiyuan 030051, China; 315559492@qq.com (M.Z.); xf_zhao@st.nuc.edu.cn (X.Z.); yjzhang@nuc.edu.cn (Y.Z.)

[2] School of Science, Jiangsu Provincial Research Center of Light Industrial Optoelectronic Engineering and Technology, Jiangnan University, Wuxi 214122, China; wangjcheng@1sdf.com

[3] Aerospace Science and Technology Corporation, Beijing Institute of Space Long March Vehicle, Beijing 100036, China; Jinwen@sdfsdf.com

* Correspondence: shubin_yan@nuc.edu.cn; Tel.: +86-351-392-0398

† These authors contributed equally to this work.

Abstract: In this study, we design a new refractive index sensor based on a metal–insulator–metal waveguide coupled with a notched ring and vertical rectangular resonators. We use the finite element method to study the propagation characteristics of the sensor. According to the calculation results, the transmission spectrum exhibits a typical Fano resonance shape. The phenomenon of Fano resonance is caused by the coupling between the wide spectrum and narrow spectrum. In the design, the wide spectrum signal is generated by the vertical rectangular resonator, while the narrow spectrum signal is generated by the notched ring resonator. In addition, we varied the structural parameters of the resonators and filled the structure with media of different refractive indices to study the sensing properties. The maximum achieved sensitivity of the sensor reached 1071.4 nm/RIU. The results reveal potential applications of the coupled system in the field of sensors.

Keywords: surface plasmon polaritons; Fano resonance; finite element method; refractive index sensor

1. Introduction

Surface plasmon polaritons (SPPs) are charge density waves [1,2] and are formed by the interference of free electrons and electrons on the surface of a metal film, which propagate along the metal surface, and the electric field amplitude decays exponentially in the vertical interface direction [3–7]. SPPs propagate only on the interface of metals and dielectrics; therefore, it can break through the traditional optical diffraction limit [8]. In addition, the size of the SPP model is small, and nanoscale optical transmission, processing, and control can be realized [9–11]. Optical devices based on SPP waveguide structures have been extensively studied, such as in filters [12–14], diodes [15–17], and optical switches [18–20].

In recent years, optical phenomena such as Fano resonance [21] and plasmon-induced transparency [22] caused by metal–insulator–metal (MIM) waveguide coupling cavities, which are sensitive to the surrounding environment, have attracted the interest of domestic and foreign researchers to study SPP sensors [23–25]. Thus, many sensors based on the MIM waveguide have been investigated and reported. These nanosensors include a MIM waveguide coupled with two silver baffles and a ring resonator [26], a gear-shaped nanocavity [21], and double rectangular resonators [27]. However, these plasmonic sensors currently exhibit low sensitivity, which is an enormous challenge to researchers.

 doi:10.20944/preprints201712.0027.v1

Peer-reviewed version available at *Sensors* **2017**, *17*, 2879; doi:10.3390/s17122879

In this study, a structure consisting of MIM waveguides coupled with the vertical rectangular and notched ring resonators was applied as a plasmonic refractive index nanosensor. The structure was distributed by the transmission spectra and magnetic H_z field with a perfectly matched layer absorbing boundary condition and was calculated by the finite element method. We varied the coupling distance between the vertical rectangular and notched ring resonators, and the external diameter of the notched ring resonator and length of the vertical rectangular resonator to study its sensing characteristics and refractive index sensitivity.

2. Model and Analytical Method

Figure 1 shows a schematic of the MIM waveguide coupled with the vertical rectangular resonator and the designed notched ring resonator. The vertical symmetry axes of the two resonators and MIM waveguide coincide with each other. The width w of the waveguide is 50 nm to ensure that the waveguide only possesses a transverse magnetic field (TM_0 mode) [28]. g represents both sides of the coupling distance between the vertical rectangular resonator and notched ring resonator. The inner diameter and external diameter of the notched ring resonator are r and R, respectively, while l represents the length of the vertical rectangular resonator.

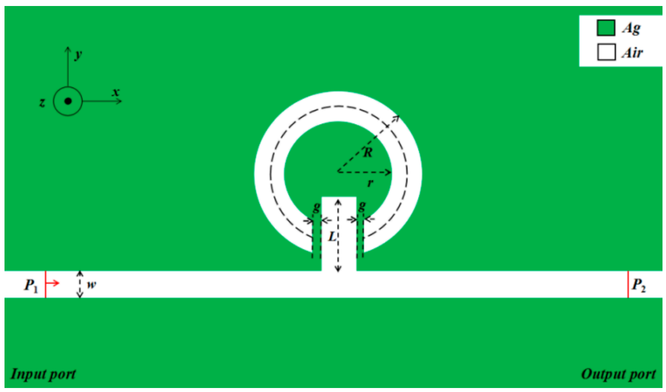

Figure 1. Two-dimensional schematic of the MIM waveguide coupled with notched ring and vertical rectangular resonators.

The white part in Figure 1 represents the MIM waveguide and resonators, the filling medium is air (dielectric constant = 1), the green part represents metallic silver, and its dielectric constant is related to the frequency of incident light. Based on the Debye–Drude dispersion model [29], the relative permittivity of silver can be defined as

$$\varepsilon(\omega) = \varepsilon_\infty + \frac{\varepsilon_s - \varepsilon_\infty}{1 + i\omega\tau} + \frac{\sigma}{i\omega\varepsilon_0} \tag{1}$$

where ε_∞ = 3.8344, τ = 7.35×10^{-15}, ε_s = −9530.5, and σ = 1.1486×10^{7} s/m are the infinite frequency permittivity, relaxation time, static permittivity, and conductivity of Ag, respectively. COMSOL Multiphysics software based on the finite element method can be applied to solve the partial differential equation, and the transmission spectra of the coupling structure under different incident light frequencies can be obtained. The transmittance is defined as $T = (S_{21})^2$, where S_{21} is the transmission coefficient from input to output (P_1 to P_2) [26].

3. Results and Discussion

In Figure 2, the transmission spectrum of the structure with R = 140 nm, r = 90 nm, l = 160 nm, n = 1 RIU, and g = 10 nm is presented. The transmittance is about 0 at λ_{dip} = 910 nm and about 0.9 at λ_{peak} = 965 nm, which is a typical Fano resonance [30] line-shape with a minimum and maximum.

Preprints (www.preprints.org) | NOT PEER-REVIEWED | Posted: 4 December 2017 doi:10.20944/preprints201712.0027.v1

Peer-reviewed version available at Sensors 2017, 17, 2879; doi:10.3390/s17122879

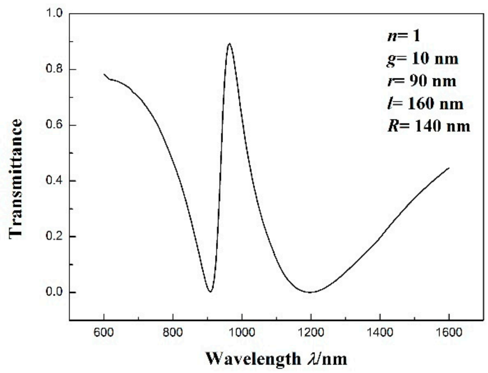

Figure 2. Transmission spectrum of the plasmonic waveguide coupling structure.

In order to better understand the internal mechanism of the change in the transmission spectra, the magnetic field distribution of the spectra at the resonance dip and peak are studied. Figures 3(a) and 3(b) show the fields *Hz* of the plasmonic waveguide-coupled system at λ_{dip} = 910 nm and λ_{peak} = 965 nm. In Figure 3(a), a weak coupling at the right side of the MIM waveguide is shown and has no SPPs coupled into it. There is a clear in-phase relationship between the lower part of the notched ring resonator and vertical rectangular resonator, and the relationship between the higher part and lower part of the notched ring resonator is anti-phase in Figure 3(b).

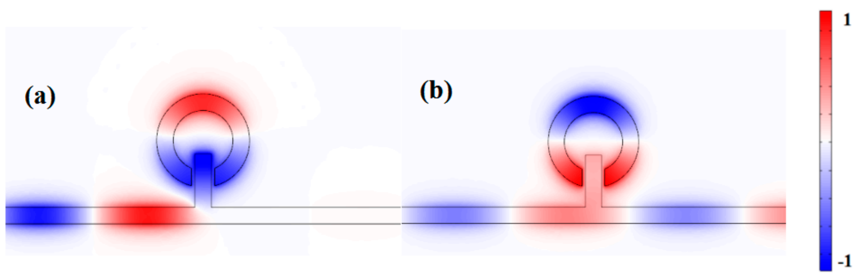

Figure 3. Contour profiles of the normalized *Hz* field of different structures at (a) λ_{dip} = 910 nm and (b) λ_{peak} = 965 nm.

Based on the propagation characteristics of the structure, the structure is applied to the refractive index sensor. The shift in the transmission spectra is due to the change in refractive index. Therefore, the shift can be defined as the sensitivity of the sensor. The effect caused by refractive index on the structure is studied by filling it with media of different refractive indices. Figure 4(a) presents the transmission spectra for different refractive indices from 1.00 to 1.05 RIU (interval of 0.01). As n increases, the transmission spectra red-shifts an equal distance. Furthermore, Figure 4(b) indicates that there is a linear relationship between the wavelength shift in the Fano resonance peak and refractive index change Δn. With the increase in n to 1.05, the Fano resonance peak shifts to 1010 nm. By linear fitting, the sensitivity $(\Delta\lambda/\Delta n)$ can be obtained. The maximum sensitivity can reach 871.4 nm/RIU. In addition, the figure-of-merit (FOM) is an important parameter for the refractive index nanosensor. It is defined as $\Delta T/(T\Delta n)$ and is 831.8 for the nanosensor.

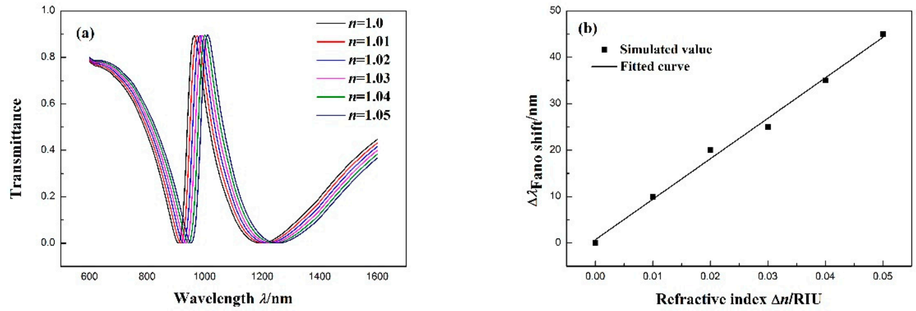

Figure 4. (a) Transmission spectra of the MIM waveguide coupled with the notched ring and vertical rectangular resonators for different n. **(b)** Fitting line of the Fano resonance peak shift ($\Delta\lambda$) with the change in refractive index (Δn).

Studying the effects of more than one coupling distance between the notched ring and vertical rectangular resonators on the Fano resonance of the structure, we find that the g factor increases from 6 to 14 nm at intervals of 2 nm while maintaining the other parameters at r = 90 nm, R = 140 nm, l = 160 nm, and n = 1 RIU. The transmittance of the Fano resonance peak increases slightly, and the position of the dip remains unchanged. In addition, the Fano resonance peak red-shifts slightly in Figure 5(a). Figure 5(b) shows the Fano resonance peak shift with the change in Δn. With the increase in n, the transmission spectra red-shifts an equal distance. The fitting calculation indicates that the maximum sensitivity can reach 928.6 nm/RIU with g = 6 and 12 nm, with FOMs of 502.1 and 681.6, respectively.

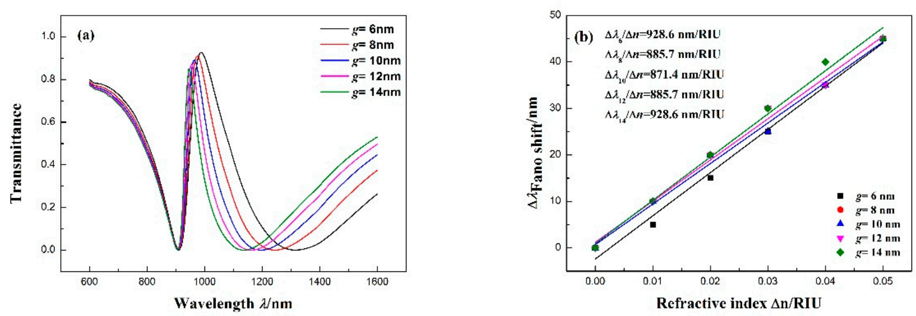

Figure 5. (a) Transmission spectra for different coupling distances g between the notched ring resonator and MIM waveguide. **(b)** Fitting line of the Fano resonance peak shift ($\Delta\lambda$) with the change in refractive index (Δn).

We also study the impact of different external diameters on the transmission spectra. The factor R increases from 120 to 160 nm at intervals while maintaining the other parameters at l = 160 nm, n = 1.00 RIU, and g = 10 nm, and the width of the notched ring is 50 nm. As shown in Figure 6(a), with the increase in the equal distance of R, the Fano resonance red-shifts an equal distance. The Fano resonance is attributed to the coupling between the wide spectrum and narrow spectrum. The wide spectrum signal is generated by the vertical rectangular resonator, while the narrow spectrum signal is generated by the notched ring resonator. The increase in R results in the growth of the narrow spectrum resonance wavelength, which leads the Fano resonance to red-shift. The fitting line of the Fano resonance peak shifts with the refractive index change (Δn) in Figure 6(b). The fitting outcome indicates that the maximum sensitivity can achieve 1071.4 nm/RIU with R = 160 nm, and its FOM is 673.6.

Preprints (www.preprints.org) | NOT PEER-REVIEWED | Posted: 4 December 2017 doi:10.20944/preprints201712.0027.v1

Peer-reviewed version available at Sensors 2017, 17, 2879; doi:10.3390/s17122879

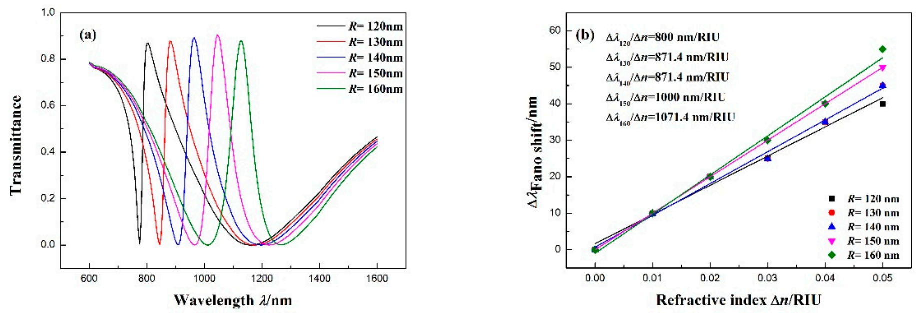

Figure 6. (a) Transmission spectra for different external diameters of the notched ring resonator *R*. **(b)** Fitting line of the Fano resonance peak shift ($\Delta\lambda$) with the change in refractive index (Δn).

Moreover, we investigated the influence of different vertical rectangular resonator lengths *l* on the transmission spectra. *l* increases from 140 to 180 nm (interval 10 nm) while maintaining the other parameters at *R* = 140 nm, *r* = 90 nm, n = 1.00 RIU, and *g* = 10 nm. As shown in Figure 7(a), with the increase in the equal distance of *l*, the transmission spectra red-shift slightly. Figure 7(b) describes the relationship of the Fano resonance peak shift with the refractive index Δn. The fitting calculation shows that the maximum sensitivity can achieve 1000 nm/RIU with *l* = 150 and 170 nm, with FOMs of 639.9 and 983.1, respectively.

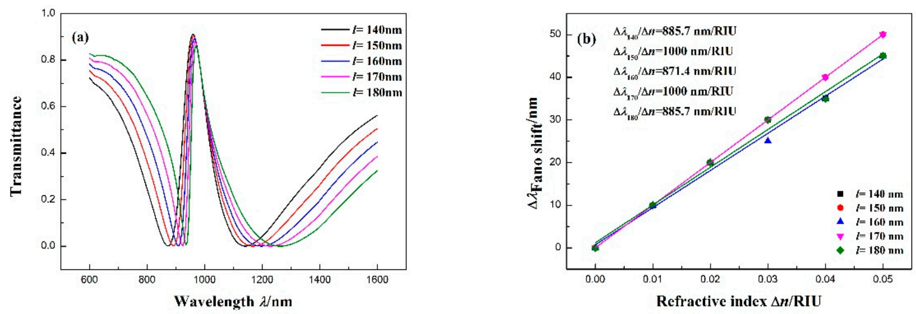

Figure 7. (a) Transmission spectra for different vertical rectangular resonator lengths *l*. **(b)** Fitting line of the Fano resonance peak shift ($\Delta\lambda$) with the change in refractive index (Δn).

4. Conclusions

We used the finite element method to study the transmission characteristics of a MIM waveguide coupled with a vertical rectangular resonator and notched ring resonator. The results indicate that the coupled structure clearly generates typical Fano resonance. Its propagation characteristics indicate that the Fano resonance in the transmission spectra depends on the geometric parameters of the notched ring resonator, and they are insensitive to small changes in the length of the vertical rectangular resonator and the coupling distance between two resonators. This characteristic significantly reduces the difficulty of the micro-/nano-processing technology. In addition, the Fano resonance produced by the structure is extremely sensitive to the change in different surrounding media, and the sensitivity reaches 1071.4 nm/RIU after optimizing the structural parameters, which provides a new method based on the MIM waveguide for detecting changes in refractive index.

Acknowledgements: This work was supported by the National Natural Science Foundation of China (Grant No.61675185), the National Science Fund for Distinguished Young Scholars (Grant No.61525107), the Natural Science Foundation of Shanxi Province (Grant No. 201601D011008).

Conflicts of Interest: The authors declare no conflict of interest.

 doi:10.20944/preprints201712.0027.v1

Peer-reviewed version available at *Sensors* **2017**, *17*, 2879; doi:10.3390/s17122879

References

1. Barnes, W. L.; Dereux, A.; Ebbesen, T.W. Surface plasmon subwavelength optics. *Nature* **2003**,*424*,824-830.
2. Zayats, Anatoly V.; Smolyaninov, I. I.; Maradudin, A. A. Nano-optics of surface plasmon polaritons, *Physics Reports* **2005**,*408*, 131-314.
3. Prasad; P. N. Nanophotonics, 2004.
4. Berini; Pierre. Surface Plasmon Nanophotonics, *Springer* **2007**,*131*,1-9.
5. Lu, H.; Liu, X.; Mao, D.; Wang, G. Plasmonic nanosensor based on fano resonance in waveguide-coupled resonators. *Optics Letters* **2012**, *37*, 3780-2.
6. Zhao, C.; Li, Y. Multiple fano resonances based on different waveguide modes in a symmetry breaking plasmonic system. *IEEE Photonics Journal* **1943**, *6*, 1-8.
7. Wu, T.; Liu, Y.; Yu, Z.; Ye, H.; Shu, C.; Peng, Y.; et al. Tuning the fano resonances in a single defect nanocavity coupled with a plasmonic waveguide for sensing applications. *Optik - International Journal for Light and Electron Optics* **2015**, *29*.
8. Gramotnev, D. K.; Bozhevolnyi, S. I. Plasmonics beyond the diffraction limit. *Nature Photonics 2010*, *4*, 83-91.
9. Yin, Y.; Qiu, T.; Li, J.; Chu, P. K. Plasmonic nano-lasers. *Nano Energy* **2012**, *1*, 25-41.
10. Zhou, N.; Ye, C.; Polavarapu, L.; Xu, Q. H. Controlled preparation of au/ag/sno2 core-shell nanoparticles using a photochemical method and applications in LSPR based sensing. *Nanoscale* **2015**, *7*, 9025-32.
11. Ozbay, E. Plasmonics: merging photonics and electronics at nanoscale dimensions. *Science* **2006**, *311*, 189.
12. Xiao, S; Liu, L; Qiu, M. Resonator channel drop filters in a plasmon-polaritons metal, *Optics Express* **2006,** *14*, 2932–2937.
13. Lin, X. S.; Huang, X. G. Tooth-shaped plasmonic waveguide filters with nanometeric sizes. *Optics Letters 2008*, *33*, 2874.
14. Xiao, B.; Kong, S.; Gu, M. Parallel coupled filter based on spoof surface plasmon polaritons. *International Conference on Optical Communications and Networks 2017* pp.1-3. IEEE.
15. Fan, C.; Shi, F.; Wu, H.; Chen, Y. Tunable all-optical plasmonic diode based on fano resonance in nonlinear waveguide coupled with cavities. *Optics Letters* **2015**, *40*, 2449-52.
16. Hu, X.; Xin, C.; Li, Z.; Gong, Q. Ultrahigh-contrast all-optical diodes based on tunable surface plasmon polaritons. *New Journal of Physics* **2010**, *12*, 023029.
17. Krummacher, B. C.; Nowy, S.; Frischeisen, J.; Klein, M.; Brütting, W. Efficiency analysis of organic light-emitting diodes based on optical simulation. *Organic Electronics* **2009**, *10*, 478-485.
18. Mao, D.; Lu, H.; Wang, L.; Liu, X.; Gong, Y. Ultrafast all-optical switching in nanoplasmonic waveguide with kerr nonlinear resonator. *Optics Express* **2011**, *19*, 2910.
19. Wang, G.; Lu, H.; Liu, X.; Gong, Y. Numerical investigation of an all-optical switch in a graded nonlinear plasmonic grating. *Nanotechnology* **2012**, *23*, 444009.
20. Y. E. Li; X. P. Zhang. Nonlinear optical switch utilizing longrange surface plasmon polaritons. *Journal of Electromagnetic Waves & Applications* **2009**, *23*, 2363-2371.
21. Zhang, Z. D.; Wang, H. Y.; Zhang, Z. Y. Fano resonance in a gear-shaped nanocavity of the metal–insulator–metal waveguide. *Plasmonics 2013*, *8*, 797-801.
22. Yan, X.; Wang, T.; Han, X.; Xiao, S.; Zhu, Y.; Wang, Y. High sensitivity nanoplasmonic sensor based on plasmon-induced transparency in a graphene nanoribbon waveguide coupled with detuned graphene square-nanoring resonators. *Plasmonics* **2016**, 1-7.
23. Kulshreshtha, R.; Zafar, R. The sensing characteristics of plasmonic waveguide with rectangular stub and taper. *International Conference on Recent Advances and Innovations in Engineering* **2017** pp.1-4. IEEE.
24. Tang, Y.; Zhang, Z.; Wang, R.; Hai, Z.; Xue, C.; Zhang, W.; et al. Refractive index sensor based on fano resonances in metal-insulator-metal waveguides coupled with resonators:. *Sensors* **2017**, *17*, 784.
25. Yun, J. G.; Kim, J.; Lee, K.; Lee, Y.; Lee, B. Numerical study on refractive index sensor based on hybrid-plasmonic mode. *International Conference on Optical Fiber Sensors* **2017** pp.103236U.
26. Zhao, X.; Zhang, Z.; Yan, S. Tunable fano resonance in asymmetric mim waveguide structure. *Sensors* **2017**, *17*.
27. Zhang, Z.; Luo, L.; Xue, C.; Zhang, W.; Yan, S. Fano resonance based on metal-insulator-metal waveguide-coupled double rectangular cavities for plasmonic nanosensors:. *Sensors* **2016**, *16*, 642-643.
28. Kekatpure, R. D.; Hryciw, A. C.; Barnard, E. S.; Brongersma, M. L. Solving dielectric and plasmonic waveguide dispersion relations on a pocket calculator. *Optics Express* **2009**, *17*, 24112-29.

Preprints (www.preprints.org) | NOT PEER-REVIEWED | Posted: 4 December 2017 doi:10.20944/preprints201712.0027.v1

Peer-reviewed version available at *Sensors* **2017**, *17*, 2879; doi:10.3390/s17122879

29. Gai, H.; Wang, J.; Tian, Q. Modified debye model parameters of metals applicable for broadband calculations. *Applied Optics* ***2007***, *46*, 2229-2233.
30. Fano, U. Effects of configuration interaction on intensities and phase shifts. *Physical Review* ***1961***, *124*, 1866-1878.